

## Validation of a Predictive Model for Corrosion inhibition of API 5L X60 Steel in Chloride Solution

K.F. Khaled<sup>1,2,\*</sup> and A. M El-Sherik<sup>3</sup>

<sup>1</sup>Materials and Corrosion Laboratory, Chemistry Department, Faculty of Science, Taif University, Saudi Arabia

<sup>2</sup>Electrochemistry Research Laboratory, Chemistry Department, Faculty of Education, Ain Shams Univ., Roxy, Cairo, Egypt

<sup>3</sup>Research and Development Center, Saudi Aramco, Dhahran, Saudi Arabia 31311

\*E-mail: [khaledrice2003@yahoo.com](mailto:khaledrice2003@yahoo.com)

*Received:* 26 November 2015 / *Accepted:* 19 December 2015 / *Published:* 1 February 2016

---

A model was previously developed to predict the corrosion inhibition efficiency of steel in chloride solutions using genetic function approximation model. The model considers the influence of steel surface, aggressive solution, surface area, volume, highest occupied and lowest unoccupied molecular orbital of the studied inhibitors and the binding energy between the steel surface and the corrosion inhibitors. The model was based on experiments carried out in the laboratory for 28 amino acids and descriptors derived from molecular dynamics simulations and quantum mechanical calculations of these inhibitors. This paper aims to develop a cross-discipline, fully integrated, quantitative model to predict the corrosion inhibition efficiency of amino acid and its related compounds (compounds that contain both amino and carboxylic groups). Experimental corrosion inhibition efficiencies have been calculated using polarization resistance measurements, potentiodynamic polarization and electrochemical impedance spectroscopy. The predicted corrosion inhibition efficiencies are compared with the experimentally determined efficiencies. The inhibition efficiencies calculated using the suggested corrosion inhibition model show good agreement with the calculated experimental corrosion inhibition efficiencies. Three new amino acid candidates are used to validate the corrosion inhibition model including N-acetylcysteine, S-methyl-L-cysteine and L-ornithine monohydrochloride.

---

**Keywords:** Electrochemical techniques; Corrosion; Molecular dynamics; Monte Carlo Simulation

### 1. INTRODUCTION

Corrosion is one of the main threats to the integrity of oil and gas pipelines. It can occur both on the inside wall and outside surface of the pipelines[1-8]. The control of corrosion is an ongoing

challenge in pipeline operations. Predicting and assuring entail the use of sensors and monitoring tools as well as predictive models[9-12].

The rich variety of corrosion inhibitor configurations which leads to many different basic properties of corrosion inhibitor molecules has continuously drawn considerable interest in corrosion science research. Computer modeling is increasingly being used as an integral part of theoretical study [13-24], in order to both test existing theories and to trigger the development of new concepts in corrosion inhibition research, computer simulations have become an essential tool in materials research, especially for predicting and understanding the behaviour of corrosion inhibitors in different corrosion systems, where a complete theory is not available. It has been proven to be an effective and inexpensive way to study these systems.

Protection of metal corrosion can be occurred through the adsorption of inhibitor molecules on the surface of the metal via the polar groups which acting as the reactive sites in these molecules. A barrier between the metal surface and the corrosion media will isolate the metal surface from the corrosive environment. The corrosion inhibition efficiency will depend on the structure of the adsorption layer as well as the experimental conditions.

Although of several experimental [25] and computational techniques that have been considered to study the inhibitor chemical and structural characteristics, there is a little known about the interaction of the inhibitor molecules with the surface of the metal. Computer simulations using suitable models is the most practical route to study corrosion inhibition process.

As corrosion system are more complex where a relatively large number of molecules are involved, the quantum chemical computing method is no longer suitable for these complex systems. Quantum chemical approach is efficient only in this complex system by making the following assumptions [26]: the inhibition efficiency depends only on the inhibitor molecule structure and everything else in the inhibitor surrounding area is uninvolved either with respect to competition for the surface or with respect to itself. Also, it is clear that there is no general approach for predicting compound usefulness to be a potentially effective corrosion inhibitor or find some universal type of correlation. A number of excluded parameters that should be included, the effect of solvent molecules, metal surface characteristics, and adsorption sites of the metal atoms or involved oxide sites or vacancies, competitive adsorption with other chemical species in the fluid phase and solubility give at least simplified inspection. In this situation, a molecular simulation method is the best choice in an attempt to take into consideration the effect of these excluded parameters[15].

## 2. COMPUTATIONAL DETAILS

Interaction between the three new compounds and Fe (1 1 1) plane surface was simulated in a simulation box of dimensions' ( $17.38 \text{ \AA} \times 17.38 \text{ \AA} \times 44.57 \text{ \AA}$ ) with periodic boundary conditions to model a representative part of the metal-inhibitor interface devoid of any arbitrary boundary effects. The Fe (1 1 1) plane surface was built and relaxed by minimizing its energy using molecular mechanics tools, then the surface area of Fe (1 1 1) was increased a super cell was constructed. A vacuum slab with  $15 \text{ \AA}$  thicknesses built on the Fe (1 1 1) surface. The number of layers in the

structure was chosen to equal four of iron atoms which was a sufficient depth that the amino acids and its derivatives will only be involved in non-bond interactions with iron atoms in the layers of the surface, without multiplication the calculation time unreasonably. This design then converted to have 3D periodicity [27, 28]. Also, it is important that the size of the vacuum slab is big enough (15 Å) that the non-bond calculations for the amino acids do not interact with the periodic image of the bottom layer of atoms in the surface. After minimizing the Fe (1 1 1) surface and the three inhibitor molecules, the corrosion system will be built to place the amino acids on Fe (1 1 1) surface, and the adsorption of these molecules on the Fe (1 1 1) surface were simulated using the COMPASS (condensed phase optimized molecular potentials for atomistic simulation studies) force field. The adsorption these amino acids on iron surface gives the energetic of the adsorption and its effects on the inhibition efficiencies of amino acid molecules[27, 28]. The binding energy between the studied amino acid molecules and Fe (111) surface were calculated using the following equation [15, 29]:

$$E_{\text{binding}} = E_{\text{total}} - (E_{\text{surface}} + E_{\text{inhibitor}}) \quad (1)$$

Where  $E_{\text{total}}$  is the total energy of the surface and inhibitor,  $E_{\text{surface}}$  is the energy of the surface without the inhibitor, and  $E_{\text{inhibitor}}$  is the energy of the inhibitor without the surface.

In the current study, the studied amino acids have been simulated as inhibitor molecules adsorbed on Fe(111) surface to locate the low energy adsorption sites on Fe(111) surface and to investigate the preferential adsorption of the studied inhibitors. Monte Carlo simulation method was used to calculate the adsorption density as well as the binding energy of the studied inhibitor molecule. In this work, possible adsorption configurations have been recognized by implementation Monte Carlo simulation searches of the configurational space of the Fe(111)/ amino acid inhibitor system as the temperature is slowly lowered. Amino acid inhibitor molecules built and their energy was minimized using Forcite classical simulation engine [30, 31]. Geometry optimization is based on decreasing the magnitude of calculated forces until they become smaller than defined convergence tolerances[30]. The forces on the atoms in the studied inhibitors are calculated from the potential energy expression and will, therefore, depend on the force field that is selected[30].

Molecular modelling of corrosion inhibitors was carried out using both Materials Studio and Hyperchem molecular modelling software marketed by Accelrys Inc., and hypercube, respectively. For each amino acid molecule a full geometry optimization performed using both PM3 –semi-empirical molecular orbital method and Density Function Theory, DFT calculations. Molecular modelling conducted to correlate fundamental binding properties with calculated quantum mechanical parameters as molecular sizes. This study was necessary as previous computational studies failed to find a clear cut definitive correlation between quantum mechanical molecular properties (i.e. dipole moments, HOMO, LUMO and energy gaps and total energy) and corrosion inhibition efficiencies of various compounds. In fact some studies have found relationships between quantum descriptors and inhibition efficiency [32-39]

### 3. EXPERIMENTAL DETAILS

The measurements were carried out using API 5L X60 steel rod mounted in Teflon with an exposed area of  $0.311 \text{ cm}^2$  used for polarization resistance, potentiodynamic polarization, and electrochemical impedance *EIS* measurements. Inhibitor compounds were obtained from Aldrich Chemical Co. It was added to the corrosive medium (1.0 M HCl) (Fisher Scientific) at concentrations of  $10^{-6}$ ,  $5 \cdot 10^{-5}$ ,  $10^{-4}$ ,  $10^{-3}$  and  $10^{-2}$  M. Only the experimental data obtained at concentration  $10^{-2}$  M was used to validate the model.

Electrochemical experiments were carried out using a conventional electrolytic cell with three-electrode arrangement: saturated Ag/AgCl reference electrode, platinum mesh as a counter electrode, and the working electrode (*WE*) had the form of a rod. The counter electrode was separated from the working electrode compartment by fritted glass. The reference electrode was connected to a Luggin capillary to minimize *IR* drop. Solutions were prepared from bidistilled water of the resistivity  $13 \text{ M}\Omega\text{cm}$ . Prior to each experiment, the specimen was polished with a series of emery papers of different grit sizes up to 4/0 grit sizes, polished with  $\text{Al}_2\text{O}_3$  (0.5 mm particle size), washed several times with bidistilled water then with acetone and dried using a stream of air. The electrode potential was allowed to stabilize 60 minutes before starting the measurements. All experiments were conducted at  $25 \pm 1 \text{ }^\circ\text{C}$ .

Polarization resistance measurements were obtained by changing the electrode potential automatically from (-20 to 20 mV vs Ag/AgCl) at open circuit potential with scan rate of  $0.1 \text{ mV s}^{-1}$ .

Potentiodynamic polarization curves were obtained by changing the electrode potential automatically from (-500 to 1.5 mV vs Ag/AgCl) at open circuit potential with scan rate of  $5.0 \text{ mV s}^{-1}$ .

*EIS* measurements were carried out in a frequency range of 100 kHz to 40 mHz with amplitude of 5 mV peak-to-peak using ac signals at open circuit potential.

Measurements were performed with a Gamry Instrument Reference 3000 Potentiostat/Galvanostat/ZRA. This includes a Gamry framework system based on the ESA400, Gamry applications that include DC105 for dc corrosion measurements, EIS300 for electrochemical impedance spectroscopy measurements to calculate the corrosion current and the Tafel constants along with a computer for collecting the data. Echem Analyst 6.11 software was used for plotting, graphing and fitting data.

For model validation, three new amino acid candidates are used including N-acetylcysteine, S-methyl-l-cysteine and L-ornithine monohydrochloride.

### 4. RESULTS AND DISCUSSION

**Table 1.** Equation Model used to calculate the predicted inhibition efficiency[40]

Equation	Definitions
$Y = -17067.664384301 * X1$	$X1 : C : E(\text{HOMO}) (\text{Ha})$
$+ 9194.528783443 * X2$	$X2 : D : E(\text{LUMO})(\text{Ha})$
$+ 0.416465461 * X4$	$X4 : F : \text{Binding Energy (Kcal/mol)}$
$+ 0.997912242 * X12$	$X12 : N : \text{Molecular volume (vdW volume) (Spatial Descriptors)}$

+ 49922.123879648 * X14	X14 : (C : E(HOMO) (Ha)) * (E : [E(LUMO)-E(HUMO)](Ha))
- 3433.185745850 * X24	X24 : (D : E (LUMO)(Ha)) * (E : [E(LUMO)-E(HUMO)](Ha))
+ 4.385840138 * X25	X25 : (D : E (LUMO)(Ha)) * (F : Binding Energy (Kcal/mol))
- 0.003332091 * X78	X78 : (M : Molecular area (vdW area) (Spatial Descriptors)) * (N : Molecular volume (vdW volume) (Spatial Descriptors))
-1507.66	

According to the corrosion inhibition model presented in Table 1[40], it has been noticed that the predicted inhibition efficiency depends on five descriptors include highest occupied molecular orbital, lowest unoccupied molecular orbital, energy gap, binding energy, molecular area and molecular volume. To validate the suggested model in Table 1, three new amino acids namely, N-acetylcysteine, S-methyl-l-cysteine and L-ornithine monohydrochloride have been selected and several electrochemical techniques have been used to determine the corrosion inhibition efficiency for those candidates at various concentrations. Those experimental electrochemical techniques include polarization resistance measurements, electrochemical impedance spectroscopy and potentiodynamic polarization. As mentioned in our previous work [40] that the corrosion inhibition efficiencies used to construct the model in Table 1 have been calculated for the amino acids at 0.01 M concentrations, we have compared the predicted inhibition efficiencies for the new amino acid candidates at 0.01M.

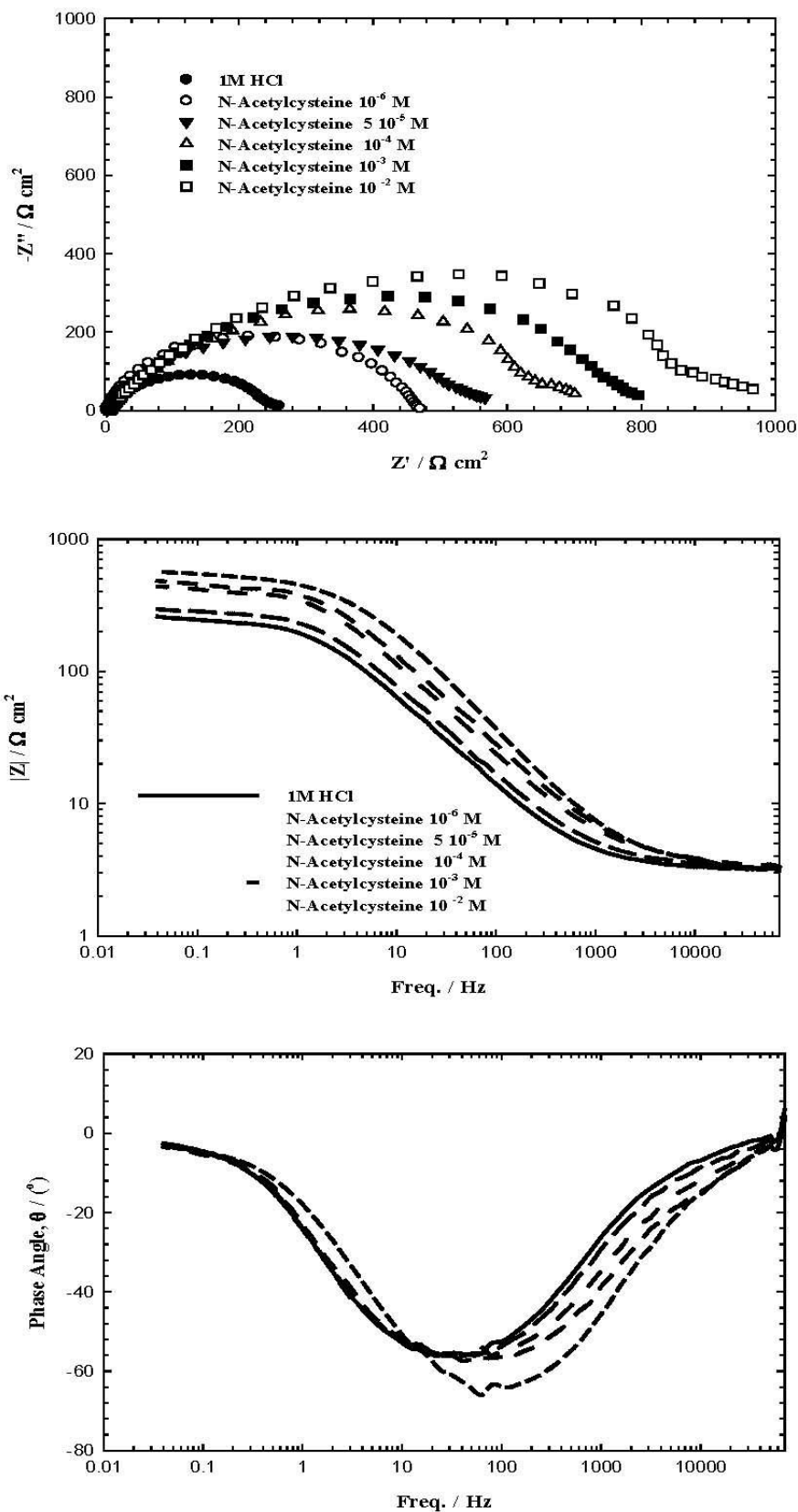
#### 4.1. Electrochemical investigations

Figure 1 (representative example) shows E-I curves for 5LX60 steel electrode in 1 M HCl solutions in absence and presence of various concentrations of N-acetylcysteine at  $25 \pm 1$  °C using polarization resistance measurements. Tables 2-4 show the electrochemical kinetic parameters and inhibition efficiencies recorded for 5LX60 in 1 M HCl solutions without and with various concentrations of N-acetylcysteine, S-methyl-l-cysteine and L-ornithine monohydrochloride at  $25 \pm 1$  °C calculated by polarization resistance measurements. As can be seen from Tables 2-4, the polarization resistance increases as the concentration increases, i.e. corrosion rate decreases and inhibition efficiency increases. Inhibition efficiency calculated from the following equation:

$$E_{R_p} \% = \left(1 - \frac{R_p^o}{R_p}\right) \times 100 \quad (2)$$

where  $R_p^o$  and  $R_p$  are the polarization resistances calculated from polarization resistance measurements for uninhibited and inhibited solutions, respectively.





**Figure 2.** EIS plots for Steel 5LX60 in 1 M HCl solutions in absence and presence of various concentrations of N-acetylcysteine at  $25 \pm 1$  °C

**Table 3.** Electrochemical kinetic parameters and inhibition efficiencies recorded for Steel 5LX60 in 1 M HCl solutions without and with various concentrations of S-methyl-l-cysteine at 25 ±1 °C calculated by polarization resistance measurements

Conc. M	R <sub>p</sub> Ω.cm <sup>2</sup>	I <sub>corr</sub> mA.cm <sup>-2</sup>	-E <sub>corr</sub> mV <sub>Ag/AgCl</sub>	E <sub>Rp</sub> %
0.00	1.036	25.14	20.36	-----
10 <sup>-6</sup>	2.342	11.13	20.28	55.76
5 10 <sup>-5</sup>	2.589	10.0	20.28	59.98
10 <sup>-4</sup>	4.503	5.785	20.29	76.99
10 <sup>-3</sup>	6.853	3.802	20.28	84.88
10 <sup>-2</sup>	12.95	2.012	20.30	92.00

**Table 4.** Electrochemical kinetic parameters and inhibition efficiencies recorded for Steel 5LX60 in 1 M HCl solutions without and with various concentrations of l-ornithine monohydrochloride at 25 ±1 °C calculated by polarization resistance measurements

Conc. M	R <sub>p</sub> Ω.cm <sup>2</sup>	I <sub>corr</sub> mA.cm <sup>-2</sup>	-E <sub>corr</sub> mV <sub>Ag/AgCl</sub>	E <sub>Rp</sub> %
0.00	1.036	25.14	20.36	-----
10 <sup>-6</sup>	1.37	18.95	20.38	24.37
5 10 <sup>-5</sup>	1.64	15.85	20.28	36.82
10 <sup>-4</sup>	1.84	14.09	20.30	43.69
10 <sup>-3</sup>	1.99	13.08	20.21	47.93
10 <sup>-2</sup>	3.04	8.55	20.30	65.92

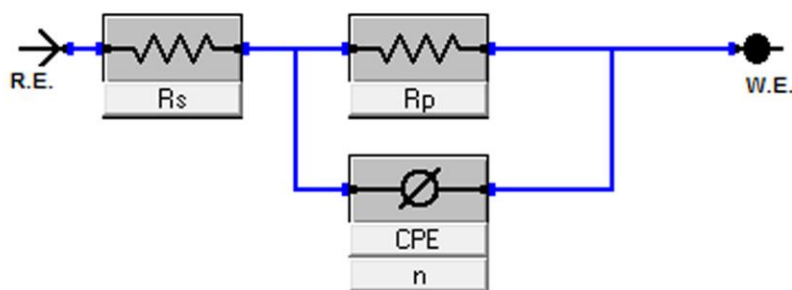


**Figure 3.** Equivalent circuit model for steel 5LX60 in 1 M HCl solutions

Results of electrochemical impedance measurements were presented in Fig. 2 (representative example) as Nyquist and Bode plots. Electrochemical impedance measurements were conducted in 1 M HCl solutions without and with different concentrations of the N-acetylcysteine. Nyquist plots presented in Fig. 2 shows compressed semicircles with the center under the real axis. This behaviour is

distinguishing for solid electrodes and often referred to as frequency dispersion and caused due to the roughness and other inhomogeneities of the steel surface [41-43]. The semicircle (capacitive loop) was related to charge-transfer in corrosion inhibition process [44]. The compressed form of the higher frequency loop reflects the surface inhomogeneity of structural or interfacial origin, such as those found in adsorption processes [45]. Equivalent circuit in Fig. 3 used to model EIS plots presented in Fig. 2. Equivalent circuit presented in Fig. 3 are proposed by several authors [46-48] in similar studies. Parameters derived from equivalent circuit in Fig. 3 and inhibition efficiency is given in Tables 5-7.

**Table 5.** Electrochemical parameters calculated from EIS measurements on steel 5LX60 electrode in 1M HCl solutions without and with various concentrations of N-acetylcesteine at  $25 \pm 1$  °C by electrochemical impedance spectroscopy.

Conc. M	$R_s$ $\Omega.cm^2$	$R_p$ $\Omega.cm^2$	$CPE$ $\mu\Omega^{-1}cm^{-2}S^n$	n	$E_{IMP}$ %
0.00	3.1	256	43.1	0.756	-----
$10^{-6}$	3.2	466	35.2	0.792	45.06
$5 \cdot 10^{-5}$	3.2	570	22.4	0.742	55.08
$10^{-4}$	3.9	697	20.1	0.775	63.27
$10^{-3}$	5.1	800.6	19.1	0.747	68.02
$10^{-2}$	6.2	910	15.4	0.738	71.86

**Table 6.** Electrochemical parameters calculated from EIS measurements on steel 5LX60 electrode in 1M HCl solutions without and with various concentrations of s-methyl-l-cysteine at  $25 \pm 1$  °C by electrochemical impedance spectroscopy.

Conc. M	$R_s$ $\Omega.cm^2$	$R_p$ $\Omega.cm^2$	$CPE$ $\mu\Omega^{-1}cm^{-2}S^n$	n	$E_{IMP}$ %
0.00	2.3	256	43.1	0.756	-----
$10^{-6}$	3.3	568	18.3	0.651	54.92
$5 \cdot 10^{-5}$	3.1	626.1	15.6	0.781	59.11
$10^{-4}$	2.9	882.9	11.3	0.689	71.00
$10^{-3}$	4.1	1828	8.1	0.700	86.00
$10^{-2}$	3.8	3657	5.6	0.730	93.00

By increasing the concentration of N-acetylcysteine, S-methyl-l-cysteine and L-ornithine monohydrochloride, the values of polarization resistance increase and the CPE values is decreased. Constant phase element, CPE with their  $n$  values  $1 > n > 0$  showed double layer capacitors with some pores [49]. The decrease in CPE results from a decrease in local dielectric constant and/or an increase in the thickness of the double layer, suggested that N-acetylcysteine, S-methyl-l-cysteine and L-ornithine monohydrochloride molecules inhibit the steel corrosion by adsorption at the steel/acid interface. The semicircles in Fig. 2 are generally associated with the relaxation of electrical double

layer capacitors and the diameters of these semicircles can be considered as the charge-transfer resistance ( $R_{ct} = R_p$ ) [50].

**Table 7.** Electrochemical parameters calculated from EIS measurements on steel 5LX60 electrode in 1M HCl solutions without and with various concentrations of l-ornithine monohydrochloride at  $25 \pm 1$  °C by electrochemical impedance spectroscopy.

Conc. M	$R_s$ $\Omega.cm^2$	$R_p$ $\Omega.cm^2$	$CPE$ $\mu\Omega^{-1}cm^{-2}S^n$	n	$E_{IMP}$ %
0.00	2.3	256	43.1	0.756	0.00
$10^{-6}$	3.3	336.7	35.6	0.759	23.96
$5 \cdot 10^{-5}$	3.1	395.8	26.7	0.771	35.32
$10^{-4}$	2.9	427.4	22.6	0.779	40.10
$10^{-3}$	4.1	455.6	18.9	0.785	43.81
$10^{-2}$	3.8	719.4	17.1	0.788	64.41

Therefore, the inhibition efficiency,  $E_{IMP}$  % presented in Tables 5-7 of N-acetylcysteine, S-methyl-l-cysteine and L-ornithine monohydrochloride for the steel electrode can be calculated from the charge-transfer resistance as follows [46]:

$$E_{IMP} \% = \left(1 - \frac{R_p^o}{R_p}\right) \times 100 \tag{3}$$

where  $R_p^o$  and  $R_p$  are the polarization resistances calculated from EIS measurements for uninhibited and inhibited solutions, respectively.

**Table 8.** Electrochemical parameters calculated from polarization measurements on steel 5LX60 electrode in 1M HCl solutions without and with various concentrations of N-acetylcysteine at  $25 \pm 1$  °C by potentiodynamic polarization measurements.

Conc. M	$I_{corr}$ $\mu A.cm^{-2}$	$-E_{corr}$ mV	$b_a$ $mV.dec^{-1}$	$-b_c$ $mV.dec^{-1}$	C.R mpy	$E_T$ %
0.00	238	426	159.6	--	108.8	----
$10^{-6}$	148.5	403	156	135.2	67.8	37.60
$5 \cdot 10^{-5}$	138.0	389	141.1	115.7	63.01	42.01
$10^{-4}$	100.0	373	143.8	92.7	45.9	57.98
$10^{-3}$	93.3.26	364	145.2	96.3	42.67	60.79
$10^{-2}$	76.3	355	151.4	88.6	34.85	67.94

**Table 9.** Electrochemical parameters calculated from polarization measurements on steel 5LX60 electrode in 1M HCl solutions without and with various concentrations of s-methyl-l-cysteine at 25 ±1 °C by potentiodynamic polarization measurements.

Conc. M	$I_{corr}$ $\mu A.cm^{-2}$	$-E_{corr}$ mV	$b_a$ $mV.dec^{-1}$	$-b_c$ $mV.dec^{-1}$	C.R mpy	$E_T$ %
0.00	238	426	159.6	--	108.8	----
$10^{-6}$	117	395.1	119.7	241.1	53.65	50.84
$5 \cdot 10^{-5}$	103.0	375.7	62.0	112.1	46.92	56.72
$10^{-4}$	81.0	360.0	102.2	77.6	36.99	65.96
$10^{-3}$	35.1	331.8	63.7	79.0	16.03	85.25
$10^{-2}$	21.9	346.2	76.1	94.2	9.99	90.79

**Table 10.** Electrochemical parameters calculated from polarization measurements on steel 5LX60 electrode in 1M HCl solutions without and with various concentrations of l-ornithine monohydrochloride at 25 ±1 °C by potentiodynamic polarization measurements.

Conc. M	$I_{corr}$ $\mu A.cm^{-2}$	$-E_{corr}$ mV	$b_a$ $mV.dec^{-1}$	$-b_c$ $mV.dec^{-1}$	C.R mpy	$E_T$ %
0.00	238	426	159.6	--	108.8	-----
$10^{-6}$	190	410	155	---	86.84	20.16
$5 \cdot 10^{-5}$	168	388	87.6	125.8	76.6	29.41
$10^{-4}$	152	382	149.4	134.2	69.3	36.13
$10^{-3}$	138	389	159.7	128	63.05	42.01
$10^{-2}$	96.9	394	162.5	218.7	44.29	59.28

Addition of N-acetylcysteine, S-methyl-l-cysteine and L-ornithine monohydrochloride reduces the cathodic and anodic currents,  $i_{corr}$  as illustrated in Figure 4.

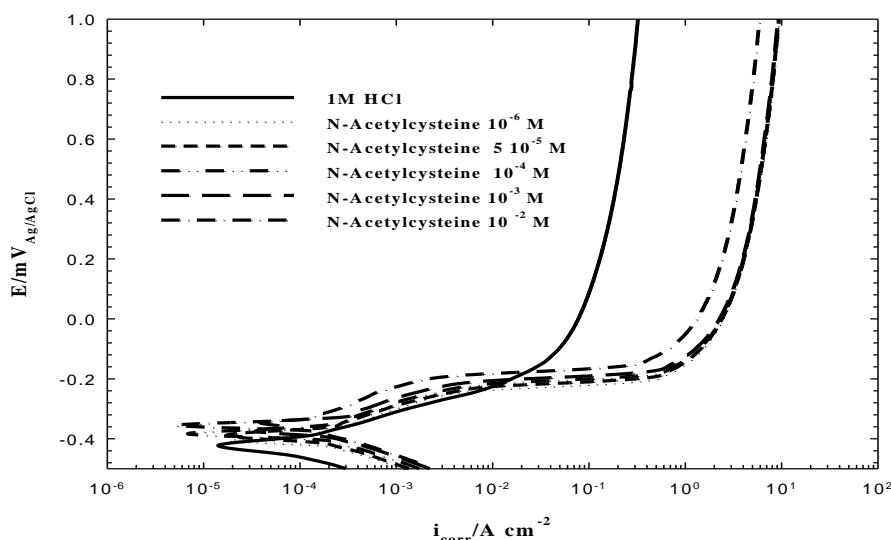


**Figure 4.** Anodic and cathodic potentiodynamic polarization curves for Steel 5LX60 in 1 M HCl solutions in absence and presence of various concentrations of N-acetylcysteine at 25 ±1 °C.

The corresponding electrochemical kinetics parameters such as corrosion potential ( $E_{\text{corr}}$ ), anodic Tafel slopes ( $b_a$ ), cathodic Tafel slopes ( $b_c$ ) and corrosion current density ( $i_{\text{corr}}$ ), obtained by extrapolation of the Tafel lines are presented in Tables 8-10. The inhibitor efficiency  $E_T\%$  was evaluated from dc measurements using the following equation [42]:

$$E_T\% = \left(1 - \frac{i_{\text{corr}}}{i_{\text{corr}}^0}\right) \times 100 \quad (4)$$

where  $i_{\text{corr}}^0$  and  $i_{\text{corr}}$  correspond to uninhibited and inhibited current densities, respectively. N-acetylcysteine, S-methyl-L-cysteine and L-ornithine monohydrochloride  $E_T\%$ .

#### 4.2 Descriptors calculations

Geometrical parameters of all stationary points for the three investigated amino acids and their related compounds are optimized in aqueous phase, employing analytic energy gradients. The generalized gradient approximation (GGA) within the density functional theory was conducted with the software package DMol<sup>3</sup> in Materials Studio of Accelrys Inc [30, 51-56]. The Becke–Lee–Yang–Parr (BLYP) exchange correlation functional and the double numerical with polarization (DNP) basis set [22, 57-59] were used in all calculations, since this was the best set available in DMol<sup>3</sup>. A Fermi smearing of 0.005 hartree and a real space cutoff of 3.7 Å was chosen to improve the computational performance. All computations were performed with spin polarization[40].

Electrochemical corrosion phenomenon takes place in the liquid phase, so it is relevant to include the effect of solvent in the computations. Self-consistent reaction field (SCRF) theory [60], with Tomasi's polarized continuum model (PCM) was used to perform the calculations in solution. These methods model the solvent as a continuum of uniform dielectric constant ( $\epsilon=78.5$ ) and define the cavity where the solute is placed as a uniform series of interlocking atomic spheres. Frontier molecular orbital distribution was obtained, at the same basis set level, to analyze the reactivity of the studied molecules[40].

Quantum chemical parameters, adsorption and binding energies are calculated by using Materials Studio 7.0 include DMol<sup>3</sup> tools, Forcite tools, Discover tools, Adsorption locator tools and Amorphous cell tools[30, 51-56], a high quality quantum mechanics computer program (available from Accelrys, San Diego, CA). These calculations employed an ab initio, local density functional (LDF) method with a double numeric polarization (DNP) basis set and a Becke–Perdew (BP) functional. Dmol<sup>3</sup> use a Mulliken population analysis [61].

**Table 11.** Application of the corrosion inhibition model on three new candidates

Inhibitor Name	EHOMO	ELOMO	ELUMO-EHOMO	Binding Energy	Area	Volume	Predicted Efficiency
N-Acetyl Cysteine	-0.225009	- 0.057527	0.167482	401.67	189.8621	145.4516	74.64768769
S-methyl L-cysteine	-0.1776	-0.0531	0.1245	443.56	169.5881	125.3054	89.86415867
L-ornithine monohydrochloride	-0.191911	-0.04269	0.149221	183.32	186.0023	137.0578	61.42998888

Table 11 shows descriptors derived from molecular dynamics simulations and quantum mechanical calculations for the three amino acids including highest occupied molecular orbital, lowest unoccupied molecular orbital, energy gap, binding energy, molecular area and molecular volume.

#### 4.3. Model Validation

The genetic function approximation (GFA) algorithm provide a new approach to the problem of building quantitative structure-activity relationship (QSAR) models. Replacing regression analysis with the GFA algorithm allows the construction of models competitive with or superior to those produced by standard techniques and makes available additional information not provided by other techniques[22]. Unlike most other analysis algorithms, GFA provides multiple models, where the populations of the models are created by evolving random initial models using a genetic algorithm [30]. GFA can build models using not only linear polynomials but also higher-order polynomials, splines, and other nonlinear functions [30].

Applying the suggested model in Table 1 , the predicted inhibition efficiency for the three amino acids candidates is comparable with the average inhibition efficiency calculated experimentally, which validate the suggested model as indicated in Table 11.

## 5. CONCLUSIONS

This study aims to encapsulate knowledge about how amino acids and its related compounds which used as corrosion inhibitors for steel in molar HCl [62, 63] perform into a structure-activity relationship (SAR) model using GFA. QSAR methods are now being used for predicting the inhibition efficiencies for corrosion inhibitors in dry laboratories. Success depends upon having data on a large number of compounds available. The computational method has proved satisfactory for the inhibition efficiency estimations.

#### ACKNOWLEDGEMENT

Authors are grateful for the financial support provided by SUADI ARAMCO, Contract no. 6600027957 titled "Using Multivariate Neural-network Analysis and Genetic Function Approximation methods to design new corrosion inhibitors for petroleum industry".

#### References

1. Q. Wang, *Anticorrosion oil pipe*, in, Jiangsu Changyuan Oil and Gas Pipe Anti-corrosion Co., Ltd., Peop. Rep. China . 2015, pp. 3pp.
2. *Chapter 6 - Production Engineering*, in: W.C. Lyons, G.J. Plisga, M.D. Lorenz (Eds.) Standard Handbook of Petroleum and Natural Gas Engineering (Third Edition), Gulf Professional Publishing, Boston, 2016, pp. 6-1-6-529.
3. J. Geske, N. Berghout, M. van den Broek, *International Journal of Greenhouse Gas Control*, 36 (2015) 175-188.

4. S. Zhen, Z. Duan, D. Sun, Y. Li, D. Gao, H. Li, *Optics & Laser Technology*, 59 (2014) 11-18.
5. A. Pfennig, H. Wolthusen, M. Wolf, A. Kranzmann, *Energy Procedia*, 63 (2014) 5762-5772.
6. A. Pfennig, M. Wolf, K. Heynert, T. Böllinghaus, *Energy Procedia*, 63 (2014) 5773-5786.
7. H. Fang, M. Duan, *Chapter 6 - Submarine Pipelines and Pipeline Cable Engineering*, in: H. Fang, M. Duan (Eds.) *Offshore Operation Facilities*, Gulf Professional Publishing, Boston, 2014, pp. e1-e181.
8. A. Pfennig, S. Schulz, A. Kranzmann, *Energy Procedia*, 37 (2013) 5754-5763.
9. R. Sooknah, S. Papavinasam, R. Winston Revie, *VALIDATION OF A PRREDICTIVE MODEL FOR MICROBIOLOGICALLY INFLUENCED CORROSION*, in: *CORROSION 2008 NACE*, New Orleans LA, 2008, pp. 17.
10. Y. Li, H. Wang, X. Zhang, G. Jiang, X. Wu, *Shiyou Huagong Yingyong*, 33 (2014) 98-102.
11. S.-d. Sun, S.-q. Mi, J. You, J.-l. Yu, S.-q. Hu, X.-y. Liu, *Wuli Huaxue Xuebao*, 29 (2013) 1192-1200.
12. A. Yousefi, S. Javadian, N. Dalir, J. Kakemam, J. Akbari, *RSC Adv.*, 5 (2015) 11697-11713.
13. N. Al-Mobarak, K. Khaled, M.N.H. Hamed, K. Abdel-Azim, N. Abdelshafi, *Arab. J. Chem.*, 3 (2010) 233-242.
14. N.A. Al-Mobarak, K.F. Khaled, O.A. Elhabibc, K.M. Abdel-Azim, *Journal of Materials and Environmental Science*, (2010).
15. K. Khaled, *Electrochim. Acta*, 53 (2008) 3484-3492.
16. K. Khaled, *Electrochim. Acta*, 54 (2009) 4345-4352.
17. K. Khaled, *Appl. Surf. Sci.*, 252 (2006) 4120-4128.
18. K. Khaled, *J. Solid State Electrochem.*, 13 (2009) 1743-1756.
19. K. Khaled, *Int. J. Electrochem. Sci.*, 3 (2008) 462-475.
20. K. Khaled, *Electrochim. Acta*, 55 (2010) 6523-6532.
21. K. Khaled, *J. Appl. Electrochem.*, 41 (2011) 423-433.
22. K.F. Khaled, *Corros. Sci.*, 53 (2011) 3457-3465.
23. K. Khaled, N. Abdel-Shafi, N. Al-Mobarak, *Int. J. Electrochem. Sci.*, 7 (2012) 1027-1044.
24. K. Khaled, N. Al-Mobarak, *Int. J. Electrochem. Sci.*, 7 (2012) 1045-1059.
25. K.F. Khaled, M.N.H. Hamed, K.M. Abdel-Azim, N.S. Abdelshafi, *J. Solid State Electrochem.*, 15 (2011) 663-673.
26. K.F. Khaled, K. Babic-Samardzija, N. Hackerman, *Electrochim. Acta*, 50 (2005) 2515-2520.
27. K. Khaled, *Appl. Surf. Sci.*, 256 (2010) 6753-6763.
28. K.F. Khaled, *J. Solid State Electrochem.*, 13 (2009) 1743-1756.
29. K. Khaled, *Appl. Surf. Sci.*, 255 (2008) 1811-1818.
30. K. Khaled, N. Abdel-Shafi, *Int. J. Electrochem. Sci.*, 6 (2011) 4077-4094.
31. O. Ermer, *Calculation of molecular properties using force fields. Applications in organic chemistry*, in: *Bonding forces*, vol. 27, Springer Berlin Heidelberg, 1976, pp. 161-211.
32. L. Li, X. Zhang, J. Lei, J. He, S. Zhang, F. Pan, *Corros. Sci.*, 63 (2012) 82-90.
33. A.Y. Musa, A.B. Mohamad, A.A.H. Kadhum, M.S. Takriff, W. Ahmoda, *Journal of Industrial and Engineering Chemistry*, 18 (2012) 551-555.
34. K. Khaled, *J. Appl. Electrochem.*, 41 (2011) 277-287.
35. X. Xie, S. Cao, L. Pan, X. Gong, K. Peng, *Anti Corros. Method M.*, 51 (2004) 101-104(104).
36. G. Bereket, C. Öğretir, Ç. Özşahin, *Journal of Molecular Structure: THEOCHEM*, 663 (2003) 39-46.
37. J. Fang, J. Li, *Journal of Molecular Structure-Theochem*, 593 (2002) 179-185.
38. V.S. Sastri, J.R. Perumareddi, M. Elboudjaini, *Corrosion inhibition - Past, present and future*, 2000.
39. J.M. Hill, J. Shen, R.M. Watwe, J.A. Dumesic, *Langmuir*, 16 (2000) 2213-2219.
40. K.F. Khaled, A. Sherik, *Int. J. Electrochem. Sci.*, 8 (2013) 9918-9935.
41. H. Ma, S. Chen, L. Niu, S. Zhao, S. Li, D. Li, *J. Appl. Electrochem.*, 32 (2002) 65-72.

42. K.F. Khaled, N.A. Al-Mobarak, *Int. J. Electrochem. Sci.*, 7 (2012) 1045-1059.
43. Zarrouk, B. Hammouti, H. Zarrok, M. Bouachrine, K.F. Khaled, S.S. Al-Deyab, *Int. J. Electrochem. Sci.*, 7 (2012) 89-105.
44. H. Ashassi-Sorkhabi, N. Ghalebsaz-Jeddi, F. Hashemaddeh, H. Jahani, *Electrochim. Acta*, 51 (2006) 3848-3854.
45. R.S. Gonçalves, D.S. Azambuja, A.M. Serpa Lucho, *Corros. Sci.*, 44 (2002) 467-479.
46. K.F. Khaled, S.S. Abdel-Rehim, G.B. Sakr, *Arab. J. Chem.*, 5 (2012) 213-218.
47. K.F. Khaled, *J. Electrochem. Soc.*, 158 (2011) S28-S28.
48. L. Han, S. Song, *Corros. Sci.*, 50 (2008) 1551-1557.
49. E.M. Sherif, S.M. Park, *Electrochim. Acta*, 51 (2006) 1313-1321.
50. K.F. Khaled, N.S. Abdel-Shafi, N.A. Al-Mobarak, *Int. J. Electrochem. Sci.*, 7 (2012) 1027-1044.
51. B. Delley, *J. Chem. Phys.*, 92 (1990) 508.
52. B. Delley, *J. Chem. Phys.*, 113 (2000) 7756.
53. K. Khaled, *Mater. Chem. Phys.*, 124 (2010) 760-767.
54. K. Khaled, A. El-Maghraby, *Arab. J. Chem.*, (2010).
55. J. Barriga, B. Coto, B. Fernandez, *Tribology International*, 40 (2007) 960-966.
56. *Accelrys to Release Enhanced Suite of Chemicals and Materials Modeling and Simulation Tools with Materials Studio(R) 4.1*, in: Business Wire, New York, United States, New York, 2006, pp. 0-n/a.
57. J. Zhang, G. Qiao, S. Hu, Y. Yan, Z. Ren, L. Yu, *Corros. Sci.*, 53 (2011) 147-152.
58. J.R. Mohallem, T. de O. Coura, L.G. Diniz, G. de Castro, D. Assafrão, T. Heine, *The Journal of Physical Chemistry A*, 112 (2008) 8896-8901.
59. J.A. Ciezak, S.F. Trevino, *The Journal of Physical Chemistry A*, 110 (2006) 5149-5155.
60. M.W. Wong, M.J. Frisch, K.B. Wiberg, *J. Am. Chem. Soc.*, 113 (1991) 4776-4782.
61. R.S. Mulliken, *J. Chem. Phys.*, 23 (1955) 1833.
62. V. Hluchan, L. Wheeler, N. Hackerman, *Werkstoffe und Korrosion*, 39 (1988) 512-517.
63. K. Babić-Samardžija, C. Lupu, N. Hackerman, A.R. Barron, A. Luttge, *Langmuir*, 21 (2003) 12187-12196.